

A Mathematical Framework for Misinformation Propagation in Complex Networks: Topology-Dependent Distortion and Control

Saikat Sur,^{1, 2, *} Rohitashwa Chattopadhyay,^{3, †} Jens Christian Claussen,^{4, ‡} and Archan Mukhopadhyay^{†5, §}

¹*Optics & Quantum Information Group, The Institute of Mathematical Sciences, HBNI, CIT Campus, Taramani, Chennai 600113, India*

²*Department of Chemical and Biological Physics & AMOS, Weizmann Institute of Science, Rehovot 7610001, Israel*

³*Department of Theoretical Physics, Tata Institute of Fundamental Research, Homi Bhabha Road, Mumbai 400005, India*

⁴*School of Computer Science, University of Birmingham, Edgbaston, B15 2TT, United Kingdom*

⁵*Department of Physics, M. S. Ramaiah University of Applied Sciences, Bengaluru 560058, India*¶

(Dated: December 24, 2025)

Misinformation is pervasive in natural, biological, social, and engineered systems, yet its quantitative characterization remains challenging due to context-dependent errors and the heterogeneous structure of real-world interaction networks. We develop a general mathematical framework for quantifying information distortion in distributed systems by modeling how local transmission errors accumulate along network geodesics and reshape each agent's perceived global state. Through a drift–fluctuation decomposition of pathwise binomial noise, we derive closed-form expressions for node-level perception distributions and show that directional bias induces only a uniform shift in the mean, preserving the fluctuation structure. This establishes a previously unreported shift-invariance principle governing error propagation in networks. Applying the framework to canonical graph ensembles, we uncover strong topological signatures of misinformation: Erdős–Rényi random graphs exhibit a double-peaked distortion profile driven by connectivity transitions and geodesic-length fluctuations, scale-free networks suppress misinformation through hub-mediated integration, and optimally rewired small-world networks achieve comparable suppression by balancing clustering with short paths. A direct comparison across regular lattices, Erdős–Rényi random graphs, Watts–Strogatz small-world networks, and Barabási–Albert scale-free networks reveals a connectivity-dependent crossover. In the extremely sparse regime, scale-free and Erdős–Rényi networks behave similarly. At intermediate sparsity, Watts–Strogatz small-world networks exhibit the lowest misinformation. In contrast, Barabási–Albert scale-free networks maintain low misinformation in sparse and dense regimes, while regular lattices produce the highest distortion across connectivities. We additionally show how sparsity constraints, structural organization, and connection costs delineate regimes of minimal misinformation. Overall, our results provide an analytically tractable foundation for understanding and controlling information reliability in complex networked systems.

I. INTRODUCTION

A coordinated response in a multi-agent system relies on each agent having an accurate estimate of the global state. In real settings, however, such accuracy is rarely achieved. Physical, biological, social, and environmental sources of noise introduce small but unavoidable errors, and understanding how these errors propagate through an interaction network is essential, especially because collective performance can be extremely sensitive to local inaccuracies. In this work, the term *misinformation* refers precisely to the deviation between the true global state and the state perceived at each agent, arising from imperfect propagation across the network rather than from Shannon-theoretic information measures. Such errors may originate unintentionally from stochastic processes

or intentionally from adversarial influences, yet their consequence on collective reliability is similar as they distort how individuals in the system perceive others.

Quantification and dynamics of misinformation have been studied across journalism, sociology, neuroscience, collective biological systems, distributed computing, and networked cyber-physical systems, but a unified mathematical understanding remains limited. Prior studies have offered domain-specific or simulation-driven insights, such as qualitative analyses of error propagation based on connectivity measures [1], error accumulation in deep neural architectures [2], and preferred interaction topologies in sociotechnical and biological settings [3]. Efforts to restrict misinformation on online platforms [4] and to characterize the spread of true versus false information in complex networks [5] provide valuable perspectives, but do not yield a general analytical framework for quantifying misinformation in distributed systems.

Information flow in any multi-agent system is fundamentally shaped by connection geometry of the network. Signals often traverse multiple intermediaries, meaning that the state perceived by an agent is a non-local func-

* saikats@imsc.res.in

† rohitashwa.chattopadhyay@tifr.res.in

‡ j.c.claussen@bham.ac.uk

§ archanmukhopadhyay.pi.ns@msruas.ac.in

¶ †Corresponding author.

tion of the network topology [6, 7]. Consequently, errors accumulate along geodesic paths, as seen in network-driven propagation phenomena [8, 9]. The efficiency of information transfer therefore depends critically on the distribution of path lengths and on the small-world properties of the network [10]. When information is represented as a real-valued field, biased errors introduce additional randomness, implying that a complete description must incorporate both intrinsic fluctuations and topological constraints.

In this article, we develop a general mathematical framework for quantifying misinformation by modeling the state propagation as a path-accumulated error process. Our framework is built on the assumption that each agent has only local access to information—that is, an agent can perceive the global state of the network solely through the states of other nodes as they arrive via error-prone paths. A central analytic result is a drift–fluctuation decomposition showing that the bias parameter influences perception purely through a uniform translation of the mean, while the fluctuation structure remains invariant. This shift-invariance property, previously unidentified in network error-propagation models, greatly simplifies the resulting misinformation measure and enables closed-form expressions for the Gaussian and delta-function limits.

Applying the framework to canonical network ensembles reveals strong and previously unreported structural effects. Most strikingly, Erdős–Rényi networks exhibit a non-monotonic misinformation profile with two well-separated local maxima, arising from the interplay between the emergence of the giant component, the distribution of geodesic distances, and the formation of short cycles. To our knowledge, this double-peaked behavior has not been documented in prior studies of information distortion on networks. In contrast, scale-free networks suppress misinformation through hub-mediated global coordination, whereas optimally rewired small-world networks suppress it by balancing strong clustering with short characteristic path lengths, consistent with rewiring effects reported in [11]. These distinct but complementary mechanisms may offer insights into the reason behind the widespread existence of hub-dominated and small-world architectures in natural and engineered information-processing systems.

Overall, our work introduces an analytically tractable framework for measuring misinformation and identifying network topologies that optimize collective reliability. This framework integrates several parameters, *viz.*, error accumulation via geodesics, network geometry, and collective perception; thereby elucidates how structures shape information fidelity in complex systems, with implications for biological networks, distributed sensing, communication systems, and socio-technical platforms.

II. NOISY INFORMATION FLOW IN BIOLOGICAL NETWORKS

Biological networks provide natural examples in which information flow is inherently noisy. This noise might often have important functional consequences. Chemotactic signaling in *E. coli* fluctuates due to stochastic ligand–receptor binding and downstream processing [12, 13]; synaptic transmission is probabilistic and exhibits variability in spike timing [14, 15]; gene regulatory networks show intrinsic noise that influences cell-fate decisions [16–18]; and immune and protein–interaction networks display variability and crosstalk that reshape collective responses [19, 20]. These systems highlight that misinformation generated by noise is unavoidable, and amplification, buffering, or redirection of such errors is governed by the structure of the network.

Neuronal networks are another example of path-induced errors. Neurons communicate via action potentials that propagate across synapses, with spike timing and firing rates encoding sensory and cognitive information. Synaptic transmission, however, is inherently noisy as spikes may fail, arrive with temporal jitter, or be distorted by background activities. Such variability might prohibit coding fidelity and lead to pathological synchrony such as epileptic seizures [14, 15, 21].

Gene regulatory networks also illustrate how misinformation can arise from intrinsic stochasticity. Transcription factors regulate gene expression through activation and repression, but low copy numbers of mRNA and proteins introduce significant fluctuations. This noise can misguide cell-fate decisions or perturb developmental pathways [17, 18, 22]. Network motifs such as feed-forward loops and negative-feedback circuits are thought to buffer against such stochasticity.

The immune system offers a further example. Receptor signaling, cytokine communication, and transcriptional responses form a distributed network that are used to discriminate self from non-self. Noisy or ambiguous signals may be amplified inappropriately, generating autoimmunity, while legitimate pathogen cues may fail to elicit a sufficient response [19, 23–25].

Finally, protein–protein interaction (PPI) networks transmit signals via cascades of binding interactions. Non-specific binding, competitive interactions, and pathway crosstalk can misroute signals. The scale-free organization of many PPI networks provides resilience against random failures but also creates vulnerabilities due to reliance on highly connected hubs [20, 26, 27].

To sum up, the above examples demonstrate that misinformation due to noise is not merely a theoretical construct but a challenge that pervades across biology. They highlight how network topology shapes the reliability of distributed information processing. This reinforce the necessity for a general framework that captures how structures amplify or suppress errors across complex systems, especially across complex networks [28, 29].

III. MODEL

Let us consider a connected network \mathcal{G} consisting of n nodes (or agents) connected through m links. The information stored at each node is represented as a multi-dimensional real vector, describing the state of that node. Our goal is to formulate a field over the network—namely, the collection of these multi-dimensional states as a function of node indices. For expository clarity, we restrict attention to a one-dimensional scalar field. A higher-dimensional vector field can always be decomposed into a collection of independent orthogonal scalar components, each of which can be treated separately within the same framework. Thus, this simplification does not reduce the scientific generality of the model—it merely allows for a cleaner presentation.

We denote the state of node i by X_i . The ensemble of node states $\{X_i\}_{i=1}^n$ is described by a random variable \mathbf{X} , which takes real values x distributed according to a probability density function (PDF) $P(x)$. To make the model analytically tractable, we assume that the state of a node can influence or propagate to another node exclusively through the shortest path connecting them. This assumption effectively constrains information flow along the shortest paths (geodesic distances) on \mathcal{G} , providing a well-defined structure for modeling dynamical or diffusion-like processes on the network.

Let us denote by $X^{(j \leftarrow i)}$ the information that the j th node perceives about the i th node, and by d_{ij} the shortest path connecting the pair (i, j) . To model the bias affecting the error—whether positive or negative—we draw from a binomial distribution, where the number of trials equals the shortest path length between the nodes. Thus, the error introduced along the path consists of d_{ij} repeated independent Bernoulli trials. In each trial, the probability of a positive error ($+\varepsilon$) is r , and the probability of a negative error ($-\varepsilon$) is $(1 - r)$. We normalize the magnitude of the error per unit path by the largest possible geodesic distance between any two nodes, which is $(n - 1)$. Accordingly, we set the magnitude of the error per unit path to be

$$|\varepsilon| = \frac{1}{n-1}. \quad (1)$$

Since $d_{ij} \leq (n - 1)$ for all (i, j) , this normalization ensures that the maximum cumulative error is bounded by

$$|X^{(j \leftarrow i)} - X_i| \leq 1. \quad (2)$$

Let u denote the number of times a positive error occurs along the d_{ij} trials; then $(d_{ij} - u)$ denotes the number of negative errors. The perceived value of X_i at node j is therefore

$$\begin{aligned} X^{(j \leftarrow i)} &= X_i + \frac{1}{n-1} [u - (d_{ij} - u)] \\ &= X_i + \frac{1}{n-1} (2u - d_{ij}). \end{aligned} \quad (3)$$

In our protocol, as we traverse each unit path (i.e., link), we select the error sign from a binomial distribution. The probability that exactly u positive errors occur in d_{ij} independent trials is

$$S(d_{ij}, r, u) = \binom{d_{ij}}{u} r^u (1 - r)^{d_{ij} - u}, \quad (4)$$

where $u \in [0, d_{ij}]$. The maximum deviation in the perceived state $X^{(j \leftarrow i)}$ occurs at the extreme cases $u = 0$ or $u = d_{ij}$, in which

$$|X^{(j \leftarrow i)} - X_i| = \frac{d_{ij}}{n-1}. \quad (5)$$

On the other hand, the error is completely nullified when $u = d_{ij}/2$, provided d_{ij} is even. (please refer to the left and the middle panel of Fig. 1 for a schematic representation of our model).

A. Quantifying Misinformation

In reality, the global state of the network is encoded in the random variable \mathbf{X} . However, because errors are introduced during propagation, this global information is perceived at the j th node as a different random variable, denoted \mathbf{X}_j . Consequently, the original PDF $P(x)$ is viewed at node j as a modified distribution $Q^{(j)}(x)$. The misinformation encountered at node j can therefore be quantified by measuring the relative distance between the true distribution $P(x)$ and the perceived distribution $Q^{(j)}(x)$. A natural and widely used metric for this purpose is the relative entropy, or Kullback–Leibler (KL) divergence [30, 31]. The KL divergence between $P(x)$ (true) and $Q^{(j)}(x)$ (perceived) is defined as

$$\begin{aligned} D_{KL}(P \parallel Q^{(j)}) &= \sum_x P(x) \ln \frac{P(x)}{Q^{(j)}(x)} \\ &= H(P, Q^{(j)}) - H(P), \end{aligned} \quad (6)$$

where $H(P)$ is the Shannon entropy of $P(x)$ and $H(P, Q^{(j)})$ is the cross-entropy that measures the coding cost of $P(x)$ under $Q^{(j)}(x)$ [31, 32]. (please refer to the right panel of Fig. 1).

To characterize the overall distortion experienced by the system, we compute the average misinformation across all nodes. The misinformation per node is defined as

$$\begin{aligned} I_M &= \frac{1}{n} \sum_{j=1}^n D_{KL}(P \parallel Q^{(j)}) \\ &= -\frac{1}{n} \sum_{j=1}^n \sum_x P(x) \ln Q^{(j)}(x) - H(P). \end{aligned} \quad (7)$$

This quantity depends on both the topology of the network \mathcal{G} and the bias parameter r in the binomial error

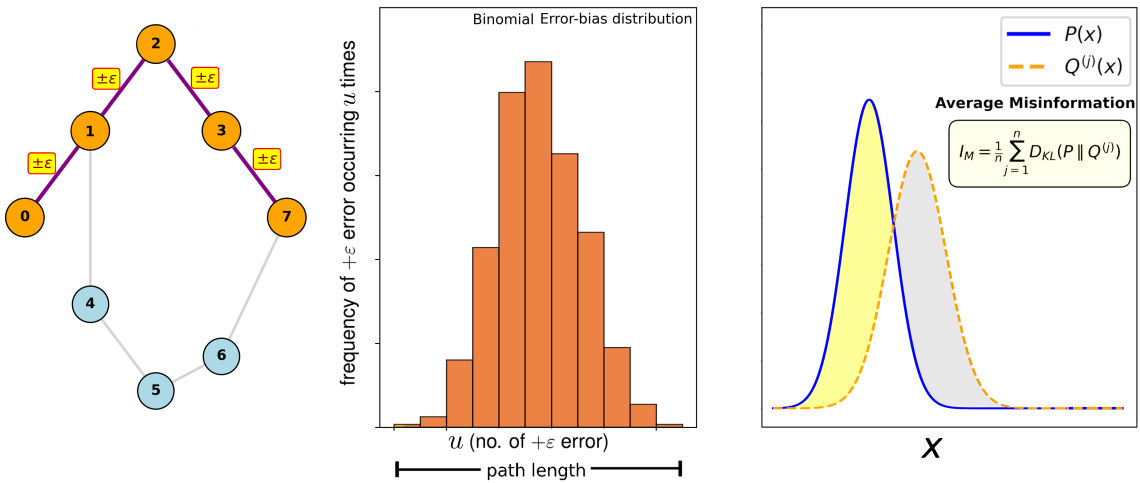


FIG. 1. **Schematic of the misinformation model.** *Left:* Illustration of error accumulation between a pair of agents in a network, where each interaction along the shortest path contributes a random error of size $\pm \varepsilon$. *Middle:* The binomial distribution of the accumulated errors. *Right:* Comparison between the true distribution $P(x)$ and the perceived distributions $Q^{(j)}(x)$, with the average misinformation quantified by the node-averaged KL divergence.

model. From Eq. 6, it is evident that misinformation reaches its maximum when the sum of cross-entropies across all nodes is maximized.

The perceived distributions $Q^{(j)}(x)$ deviate from the true distribution $P(x)$ due to the accumulation of errors. In the limit of large networks ($n \rightarrow \infty$), the distributions become continuous and the summations are replaced by integrals

$$I_M = -\frac{1}{n} \sum_{j=1}^n \int dx P(x) \ln \left(1 + \frac{Q^{(j)}(x) - P(x)}{P(x)} \right) \quad (8)$$

In this article, however, we ultimately focus on cases where the true state distribution $P(x)$ is sharply localized and approaches a Dirac delta distribution. This limit corresponds to systems in which the global state is precisely defined and all misinformation arises strictly from propagation errors rather than intrinsic variability. Before analyzing this limit, we illustrate Eq. 8 for a smooth distribution. For this purpose, we consider a Gaussian

$$P(x) = \frac{1}{\sqrt{2\pi\sigma^2}} \exp \left[-\frac{x^2}{2\sigma^2} \right], \quad (9)$$

with zero mean and standard deviation σ . With this choice, under mean-field approximation, the value of misinformation estimates to (see App. A for details)

$$I_M \approx \frac{A}{2\sigma^2} + \frac{B}{4\sigma^4}, \quad (10)$$

where the mean-field coefficients A and B depend on the distance statistics of the network and satisfy $0 < A, B < 1$. One can notice that the misinformation measure vanishes in the large-variance limit as the extremal distortion is determined solely by the variance of the Gaussian distribution. This means that when the intrinsic

uncertainty of the global state dominates over network-induced biases, the topology is irrelevant. When the true distribution is broad and unstructured, finite perception errors cannot be distinguished, and the network ceases to act as an ‘‘information-distorting medium’’. As $\sigma \rightarrow 0$ in Eq. 10, this bound diverges, implying that the Dirac-delta limit is ill-defined in this coarse-grained formalism and therefore requires a separate treatment.

For non-Gaussian integrable and nonnegative PDFs, the estimate no longer reduces to a simple closed-form expression, but it can be evaluated, in principle, from Eq. 8. On the other hand, complete networks admit a closed-form solution due to their uniform connectivity. These two special cases—the Dirac delta distribution and the complete graph topology are examined in the following sections.

IV. COMPLETE GRAPH TOPOLOGY

The true distribution $P(x)$ can be expressed in discrete form as [33]

$$P(x) = \sum_k P(x_k) \delta(x - x_k), \quad (11)$$

where the set $\{x_k\}$ denotes the discrete support points of the distribution, and the weights $P(x_k)$ satisfy the normalization condition $\sum_k P(x_k) = 1$.

In a complete graph, the shortest-path length between any two distinct nodes is unity. Hence, the error accumulated during the propagation of information from node i to node j consists of a single Bernoulli trial. The per-

ceived distribution $Q^{(j)}(x)$ at any node j is therefore

$$\begin{aligned} Q^{(j)}(x) = & f \sum_k P(x_k) \delta\left(x - x_k - \frac{1}{n-1}\right) \\ & + (1-f) \sum_k P(x_k) \delta\left(x - x_k + \frac{1}{n-1}\right) \\ & + \frac{1}{n} \sum_k P(x_k) \delta(x - x_k), \quad \forall j. \end{aligned} \quad (12)$$

Here, f denotes the fraction of the $(n-1)$ incoming states (from nodes other than j) that introduce a positive error. The first two terms represent the shifts $(x_k \rightarrow x_k + \frac{1}{n-1})$ and $(x_k \rightarrow x_k - \frac{1}{n-1})$ arising from the stochastic error process. The final term corresponds to the self-state of node j , which is perceived without distortion.

To analyse the behaviour of misinformation as the network size grows, observe that the shift magnitude $1/(n-1)$ vanishes in the limit $n \rightarrow \infty$. Consequently, the shifted measures converge to the original distribution $P(x)$. Moreover, by the law of large numbers, the empirical fraction f converges to the Bernoulli bias parameter r . Thus, in the continuum limit the perceived distribution becomes indistinguishable from the true distribution:

$$Q^{(j)}(x) \rightarrow P(x), \quad \text{as } n \rightarrow \infty. \quad (13)$$

Because the KL divergence between identical distributions is zero [31, 32], we obtain

$$D_{KL}(P \| Q^{(j)}) \rightarrow 0 \quad \text{for all } j, \quad (14)$$

which implies that the misinformation per node satisfies

$$I_M \rightarrow 0, \quad \text{as } n \rightarrow \infty. \quad (15)$$

This behaviour is a direct consequence of the normalization scheme introduced earlier, in which the maximum possible error is bounded by unity. Because the error contribution per link decays as $1/(n-1)$, a complete graph becomes “too well connected” for misinformation to accumulate in large networks. Even a biased error process in this case cannot propagate over a sufficiently long distance to produce a macroscopic distortion of the global distribution.

V. ANALYTICAL CASE STUDY OF A DIRAC-DELTA TRUE STATE

In this section, we begin with a general network in which all nodes share an identical state, say a . In this case, the true-state probability density function reduces to a Dirac distribution,

$$P(x) = \delta_{x,a}. \quad (16)$$

For analytical convenience, we assume unbiased errors, $r = \frac{1}{2}$, so that the probabilities of positive and negative

errors are equal, as in Eq. 4. Under this protocol, node j can perceive the state of node i without distortion, but only when the shortest path between them has even length. Accordingly, the perceived distribution $Q^{(j)}(x)$ decomposes as

$$\begin{aligned} Q^{(j)}(x) &= Q^{(j)}(x = a) + Q^{(j)}(x \neq a) \\ &= \frac{1}{n} \left[1 + \sum_{m \in 2\mathbb{Z}_{\geq 0}} S\left(m, \frac{1}{2}, \frac{m}{2}\right) b_m^{(j)} \right] \delta_{x,a} + Q^{(j)}(x \neq a), \end{aligned} \quad (17)$$

where $b_m^{(j)}$ denotes the number of nodes at shortest-path distance m from node j . Evaluating the above expression at $x = a$ yields

$$Q^{(j)}(a) = \frac{1}{n} \left[1 + \sum_{m \in 2\mathbb{Z}_{\geq 0}} S\left(m, \frac{1}{2}, \frac{m}{2}\right) b_m^{(j)} \right]. \quad (18)$$

The KL divergence between the true and perceived distributions is then

$$D_{KL}(P \| Q^{(j)}) = \log n - \log \left[1 + \sum_{m \in 2\mathbb{Z}_{\geq 0}} S\left(m, \frac{1}{2}, \frac{m}{2}\right) b_m^{(j)} \right]. \quad (19)$$

Averaging over all nodes gives the misinformation per node,

$$I_M = \log n - \frac{1}{n} \sum_{j=1}^n \log \left[1 + \sum_{m \in 2\mathbb{Z}_{\geq 0}} S\left(m, \frac{1}{2}, \frac{m}{2}\right) b_m^{(j)} \right]. \quad (20)$$

The second term in Eq. 20 depends entirely on the network topology and on the statistics of error propagation. Therefore, an optimal topology—one that minimizes, maximizes, or stabilizes the misinformation—must satisfy

$$\sum_{j=1}^n \Delta \log \left[1 + \sum_{m \in 2\mathbb{Z}_{\geq 0}} S\left(m, \frac{1}{2}, \frac{m}{2}\right) b_m^{(j)} \right] = 0, \quad (21)$$

where Δ denotes variations induced by infinitesimal (or discrete) changes in the shortest-path distribution $b_m^{(j)}$. Although Eq. 21 is exact, closed-form optimality conditions arise only under additional structural assumptions.

For distance-regular graphs—whose geodesic-shell structure is fully characterized by an intersection array [34]—the shell occupations $b_m^{(j)}$ are independent of j , reducing Eq. 21 to

$$\sum_{m \in 2\mathbb{Z}_{\geq 0}} S\left(m, \frac{1}{2}, \frac{m}{2}\right) \Delta b_m = 0, \quad (22)$$

which depends solely on the coefficients of the intersection array. For asymptotically tree-like networks (e.g.,

Erdős–Rényi graphs [35] or configuration models [36]), b_m admits the closed-form approximation $b_m \approx c^m$ for mean branching factor c , leading to the analytic extremality condition

$$\sum_{m \in 2\mathbb{Z}_{\geq 0}} m S\left(m, \frac{1}{2}, \frac{m}{2}\right) c^{m-1} = 0. \quad (23)$$

More generally, since $b_m^{(j)} = (A^m \mathbf{1})_j$, the spectral decomposition of the adjacency operator [37] yields the closed-form spectral condition

$$\sum_{m \in 2\mathbb{Z}_{\geq 0}} S\left(m, \frac{1}{2}, \frac{m}{2}\right) \sum_k m \lambda_k^{m-1} (\mathbf{v}_k^\top \mathbf{1})^2 = 0, \quad (24)$$

where λ_k and \mathbf{v}_k are the eigenvalues and eigenvectors of A . Thus, fully explicit optimality criteria arise whenever the geodesic structure of the network can be written in closed form—either through distance-regularity, asymptotic tree-likeness, or spectral symmetry.

VI. NUMERICAL RESULTS

To complement the analytical results of Sec. V, we performed numerical experiments on three canonical network ensembles: Erdős–Rényi (ER) random graphs, Watts–Strogatz (WS) small-world networks, and Barabási–Albert (BA) scale-free networks. For each ensemble, we computed the misinformation I_M defined in Eq. 7, averaging over *twenty-five* independent realizations. Unless stated otherwise, all simulations used $n = 5000$ nodes, and the perception distributions $Q^{(j)}(x)$ were sampled with a bin width $W \approx 2/(n-1)$ to resolve the error-induced deviations accurately. For finite networks, the perceived distributions $Q^{(j)}(x)$ must be estimated using histograms. Because the maximum error accumulated along any path in a complete graph is $\pm 1/(n-1)$, the histogram bin width should be chosen to resolve this scale. In practice, a bin width of order $W \approx 2/(n-1)$ captures the full range of error-induced shifts without excessive smoothing. Larger bins mask small deviations and underestimate misinformation, whereas bins that are too fine lead to sparse counts and noisy estimates of $Q^{(j)}(x)$.

To enable a viable comparison across networks with different structural properties, we normalize the misinformation by the maximum possible value achievable under the protocol. The normalized misinformation per node is therefore

$$I_M = \frac{\frac{1}{n} \sum_{j=1}^n D_{KL}(P \| Q^{(j)})}{\mathcal{I}}, \quad (25)$$

where we choose $\mathcal{I} = \log n$ for all the plots as this is a natural choice evident from Eq. 20.

These three topologies were chosen because they span distinct geometric and dynamical regimes relevant to

stochastic error propagation. Erdős–Rényi graphs represent maximally random connectivity, with approximately Poissonian degree fluctuations [38, 39]. Watts–Strogatz networks interpolate between regular lattices and random graphs, capturing the coexistence of short paths and high clustering that shapes diffusion and communication processes [10, 40]. Barabási–Albert networks produce heterogeneous, hub-dominated structures through preferential attachment, resulting in heavy-tailed degree distributions and nontrivial transport pathways [41, 42]. Because these ensembles differ sharply in geodesic organization, clustering, and degree heterogeneity, they induce markedly different patterns of error accumulation and dissipation. Together, they provide a representative cross-section of the topological regimes in which misinformation dynamics typically exhibit nonlinear amplification, suppression, or saturation behaviors.

A. Erdős–Rényi Networks

For Erdős–Rényi (ER) graphs $\mathcal{G}(n, p)$, we considered networks with $n = 5000$ nodes and varied the link probability p , giving an average degree $\langle k \rangle = np$ [38, 43]. Although few real-world systems follow a pure ER structure, the model is widely used as a null ensemble when links can be approximated as forming independently with equal probability p [38, 43]. Such approximations arise in relatively homogeneous settings, including classroom social networks [44], local peer-to-peer wireless setups [45], and laboratory collaboration groups [40]. Similarly, locally dense neuronal microcircuits exhibit partially random synaptic connectivity with experimentally observed connection probabilities of 5%–30% [46–48]. For networks of size $n \sim 10^3$, these values correspond to link probabilities $p \approx 0.05$ –0.3, yielding mean degrees in the range $\langle k \rangle \sim 50$ –300, consistent with empirical densities. Although real systems also display clustering and spatial constraints, they are typically sparse with roughly probabilistic links, making the ER model a natural and widely used baseline for comparison.

Figure 2 reveals a striking feature of the Erdős–Rényi network—the normalized misinformation exhibits a strongly non-monotonic dependence on the link probability, with two distinct local maxima appearing in the sparse regime. For the sparsest connected graphs, the misinformation begins at a high value and then drops rapidly to a shallow minimum just above the connectivity threshold, where the network remains almost tree-like and supports only a single long path between most node pairs, limiting the accumulation of errors. As the link probability increases further, additional edges shorten some geodesics while still preserving many long routes; this coexistence leads to a second, smaller maximum at slightly higher connectivity, reflecting amplification of path-accumulated binomial errors. Beyond this regime, the Erdős–Rényi network becomes progressively more connected, and the average shortest path collapses

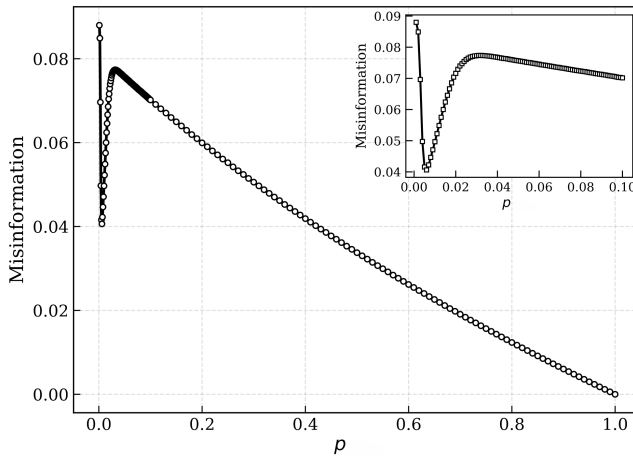


FIG. 2. **Normalized misinformation (I_M) as a function of the link probability (p) for an Erdős–Rényi network with $n = 5000$ nodes and a delta-distributed true state.** The curve begins at a high misinformation level for the sparsest connected graphs and then drops rapidly to a shallow minimum ($I_M \approx 0.04$) immediately above the connectivity threshold, where the network remains almost tree-like and limits error accumulation. As p increases further, I_M rises again to a second, smaller peak around $p \approx 0.031$, reflecting the coexistence of long geodesic paths and emerging short cycles. Beyond this point, misinformation decreases monotonically, approaching zero as $p \rightarrow 1$, where uniformly short paths strongly suppress accumulated binomial errors. This overall pattern highlights a distinct double-peaked, non-monotonic dependence of misinformation on network density.

toward its logarithmic limit [49]. This causes the misinformation to decrease monotonically and eventually approach zero when the network is fully connected. Thus, the largest distortions arise not at high connectivity but within a specific sparse range where information spreads widely yet still traverses error-prone long paths. This result is a structural feature emerging naturally from our model and, to our knowledge, not previously reported.

B. Watts–Strogatz Networks

While Erdős–Rényi graphs provide a useful baseline, their lack of clustering and structural heterogeneity limits their relevance for most real-world systems. Empirical studies across social, biological, and technological domains consistently show high clustering, modular organization, heterogeneous degree distributions, and short characteristic path lengths [10, 41, 50–52]. These features fall outside the ER framework and motivate the use of more structured generative models. The Watts–Strogatz (WS) model [10] captures the emergence of small-world structure by randomly rewiring edges in a regular lattice with probability β . This parameter controls the balance between local clustering and global integration: $\beta = 0$ produces a highly clustered ring lattice with long path

lengths, increasing β introduces shortcuts that rapidly reduce these lengths yet largely preserving local neighborhoods, and $\beta = 1$ corresponds to a random graph with very low clustering.

Small-world patterns are widely observed across biological systems, although the underlying networks are not explicitly formed by rewiring. Neural connectomes, protein–interaction and gene-regulatory networks, metabolic pathways, and ecological food webs exhibit high clustering paired with short paths [20, 26, 27, 53–56]. Comparisons with WS reference networks suggest that many biological systems occupy an intermediate effective rewiring regime, typically $\beta \approx 0.01–0.2$ [57–60]. Table I lists effective rewiring values inferred from such empirical comparisons.

Figures 3 show that misinformation depends jointly on the number of nearest neighbors and the amount of rewiring. A small amount of randomness produces the lowest misinformation, defining a narrow small-world regime in which long-range shortcuts substantially reduce path lengths while local clustering remains intact. Very low rewiring yields a highly ordered lattice where information spreads diffusively and errors accumulate along long routes. Conversely, excessive rewiring erodes the intermediate-scale organization that buffers local fluctuations, causing the network to behave more like a random graph with noise-amplifying interactions. This competition between structural order and topological randomness explains the observed non-monotonic dependence of misinformation on β .

Within this transition, an intermediate rewiring level forms an effective critical regime: local neighborhoods remain coherent, while a modest number of shortcuts provide efficient long-range coordination and suppress error accumulation [10, 61]. This crossover from diffusion-dominated to shortcut-mediated transport mirrors phenomena in disordered media and complex networks [62, 63]. Consequently, the minimum misinformation arises from the interplay between local structure (set by nearest neighbors) and the partial randomness introduced by rewiring, a balance that supports robust and efficient information flow in many natural and engineered systems.

C. Barabási–Albert Networks

Scale-free networks generated by the Barabási–Albert (BA) preferential attachment model [41] provide a natural framework for examining the role of heterogeneous connectivity in misinformation. In this model, each newly added node attaches to m existing nodes with probability proportional to their degrees, producing a power-law degree distribution

$$P(k) \sim k^{-\gamma}, \quad \gamma \approx 3, \quad (26)$$

and yielding a small number of highly connected hubs alongside many low-degree nodes. Because each new node introduces exactly m edges, the total number of

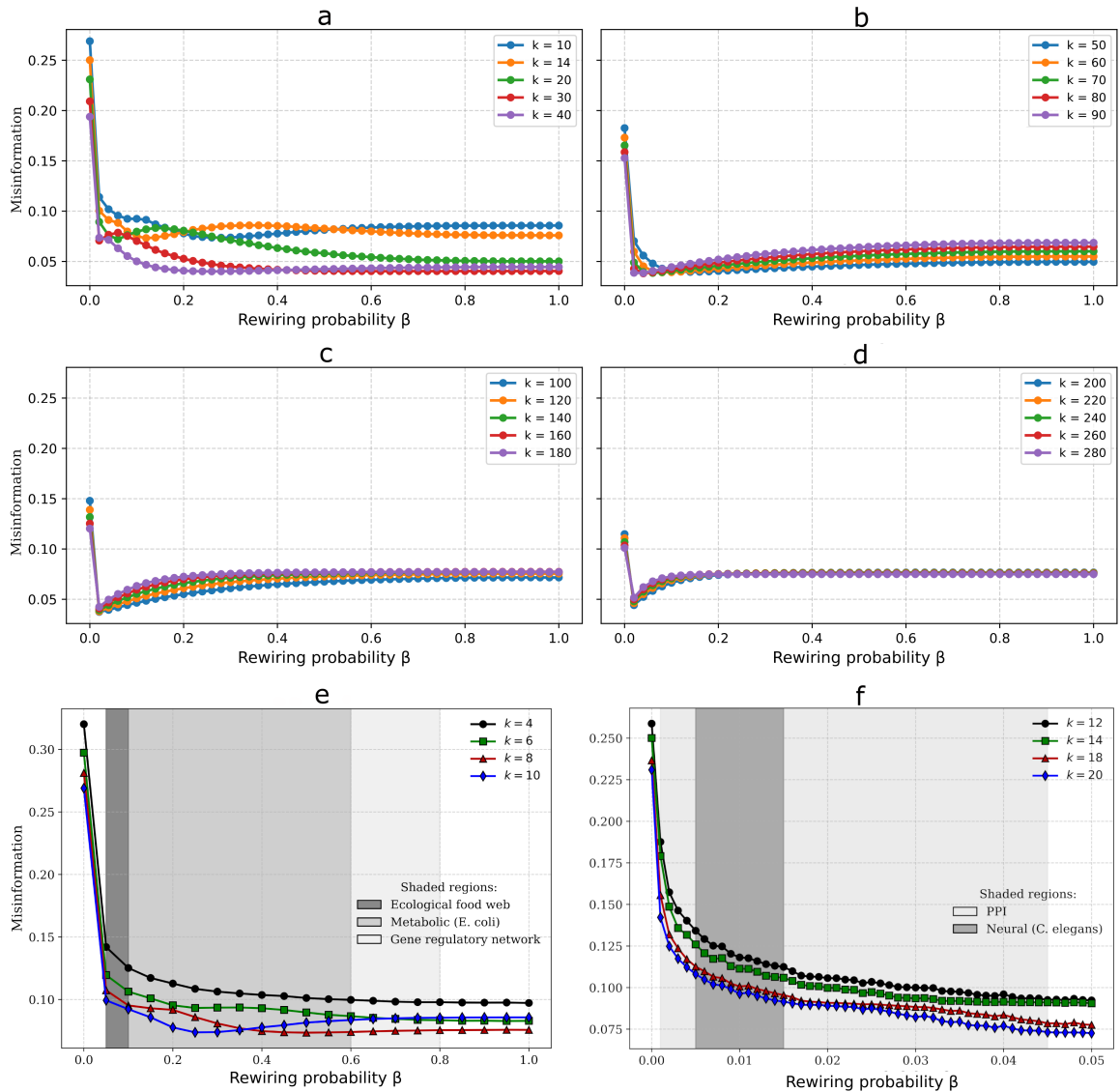


FIG. 3. Normalized misinformation (I_M) as a function of the rewiring probability for Watts–Strogatz networks with $n = 5000$ nodes and a delta-distributed true state, shown for different average degrees (panels a–d). The curves exhibit a clear non-monotonic trend: misinformation is highest in the highly ordered lattice (very low rewiring), decreases to a minimum at a small intermediate level of randomness, and then rises again before saturating in the fully randomized regime. This narrow small-world region balances local order with a few long-range shortcuts—enough to enable efficient communication while still permitting paths long enough for error accumulation—whereas both very ordered and highly randomized networks show elevated misinformation relative to this intermediate optimum. Panels (e) and (f) show the regimes occupied by real-world small-world networks and their corresponding misinformation levels, based on the effective rewiring estimates reported in Table I.

edges grows linearly with network size, giving an exact average degree $\langle k \rangle = 2m$. This heavy-tailed structure captures an organizational pattern observed broadly in biological and technological systems.

The biological relevance of scale-free architecture is well documented. Metabolic networks [67, 68], gene-regulatory circuits [74, 75], and protein–protein interaction networks [26, 27] all display degree exponents

between 2 and 3. In such systems, hubs frequently correspond to essential components—such as ATP in metabolism or master transcriptional regulators—that coordinate activity across multiple pathways and support robust communication. For context, Table II compares several biological scale-free networks with a BA network of matched average degree. Although empirical exponents vary across the range 2–3, the BA model consis-

Biological network	Size N	Half-degree $k/2$	Path length L	Effective β	Interpretation aligned with our results
Neural (<i>C. elegans</i>)	$\sim 3 \times 10^2$	5–7	2.5–3.0	0.005–0.015	Strongly ordered regime with a steep drop in misinformation even at very low β , matching the fast-decay behavior predicted by our ordered-network theory.
Metabolic (<i>E. coli</i> , human)	$\sim 10^3$	1–3	2.9–3.2	0.05–0.6	Almost-ordered to random regime; misinformation shows a slow, nearly monotonic decrease—consistent with the gradual, hub-moderated suppression predicted for low-degree biological networks.
Gene regulatory networks	10^3 – 10^4	1–3	3–4	0.04–0.8	Traverses ordered to random regimes depending on organism and condition; misinformation decays weakly due to sparse connectivity and localized regulatory motifs.
Protein–protein interaction (PPI)	10^3 – 10^5	4–10	3–5	0.001–0.045	Deeply ordered regime dominated by hub-centric architectures; predicts a sharp decline in misinformation with increasing β , consistent with strong hub buffering seen in large PPIs.
Ecological / food-web networks	10^2 – 10^3	~2–3	2.5–4	0.02–0.1	Almost-ordered to moderately random regime; misinformation remains nearly constant with a shallow decline, reflecting low connectivity and trophic modularity.

TABLE I. Approximate effective rewiring probabilities (β) for representative biological networks, obtained by matching empirical characteristic path lengths (L) to Watts–Strogatz predictions [64, 65]. The resulting interpretations show how biological systems occupy ordered, intermediate, or random topological regimes—mirroring the misinformation behaviors observed in our simulations.

Biological system	Example hubs	Functional role	γ	BA m
Metabolic network (<i>E. coli</i>)	ATP, NADH, H_2O , CO_2	Hub metabolites act as universal biochemical carriers that integrate multiple pathways, stabilize global flux balance, and buffer stochastic fluctuations arising from local reaction noise [67].	2.2–2.4	3–5
Gene-regulatory network	p53, NF- κ B	Master transcription factors regulate many downstream targets, enforce coordinated responses, maintain expression stability, and reduce error propagation in regulatory cascades [68].	2.1–2.5	1–2
Protein–protein interaction (PPI) network	Kinases, chaperones	Highly connected proteins integrate signaling modules, buffer proteomic perturbations, stabilize folding environments, and prevent miscommunication within interaction pathways [27].	2.4–2.7	3–6
Neuronal connectome	Thalamus, precuneus, rich-club hubs	High-degree cortical hubs support long-range integration, enable rapid routing between distributed brain modules, and mitigate noise accumulation in multi-step communication processes [69].	2.0–2.3	20–40

TABLE II. Representative biological scale-free networks with example hubs, functional roles relevant to misinformation suppression, and their characteristic degree-distribution exponents γ and approximate Barabási–Albert parameter m ($\langle k \rangle \approx 2m$). Neuronal ranges vary due to differences in connectome resolution, parcellation, and thresholding across datasets [70–73].

tently produces an exponent close to 3.

Turning to our numerical results, Fig. 4 shows that misinformation in BA networks depends non-monotonically on the attachment parameter m . For

small values of m , misinformation decreases rapidly: each additional edge enhances long-range communication and reduces the depth of error-prone paths. Beyond an intermediate connectivity level, misinformation begins to rise

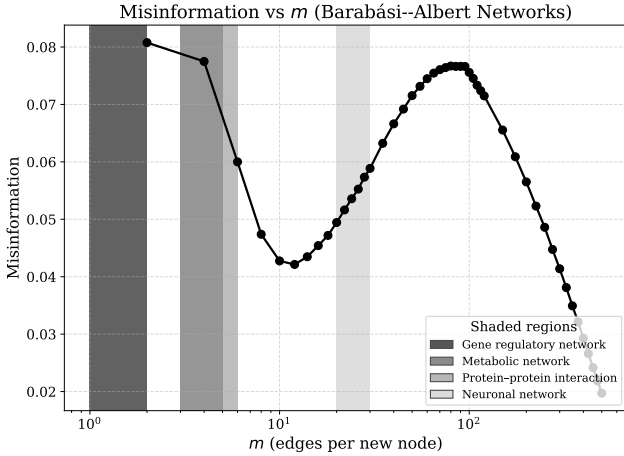


FIG. 4. **Normalized misinformation (I_M) versus the number of edges added per new node (m) in Barabási-Albert networks with $n = 5000$ nodes and a δ -distributed true state.** Misinformation initially decreases monotonically with increasing m , reflecting the well-known role of hubs in enhancing robustness and stabilizing information flow in scale-free structures [41, 62, 66]. Beyond an intermediate threshold, however, misinformation increases again, indicating a regime in which hub-driven fluctuations accumulate and propagate through the network. In the extremely sparse limit (small m), BA networks outperform random and small-world networks of comparable density, owing to their highly connected hubs, which act as efficient integrators and provide redundant communication pathways. Shaded regions show the regimes occupied by real-world scale-free networks and their corresponding misinformation levels, based on the comparable connectivity estimates reported in Table II.

again and eventually saturates, reflecting the interplay between shortened geodesics and the heterogeneous load concentrated on hubs.

D. Hierarchy of network topologies under error-propagation

A notable outcome of our analysis is that the relative performance of ER, WS, and BA networks varies with sparsity, revealing *four distinct regimes* (see Fig. 5):

(a) In the *extremely sparse regime* ($\langle k \rangle/n \lesssim 0.008$)—where the network is barely connected, our results suggest that BA networks tend to exhibit the lowest misinformation among the four canonical topologies. In this limit, ER and BA behave similarly: both reduce to thin branching structures in which misinformation grows slowly with connectivity, while the presence of a few BA hubs may provide additional local aggregation that slightly suppresses fluctuations. WS networks, by contrast, remain dominated by regular-lattice behavior at very low rewiring and thus can suffer from long path lengths that accumulate more error.

(b) As connectivity increases into the *low to intermediate regime* ($0.008 \lesssim \langle k \rangle/n \lesssim 0.052$), a surprising crossover appears: WS networks begin to outperform BA networks and achieve the minimum misinformation. WS graphs enter the small-world regime early; moderate increases in degree introduce many shortcuts without yet producing the highly heterogeneous hub structure characteristic of BA networks. This combination of short path lengths and relatively uniform degrees appears to delay the onset of error accumulation.

(c) In the regime of intermediate–high connectivity ($0.052 \lesssim \langle k \rangle/n \lesssim 0.14$), the ordering becomes such that BA networks again tend to exhibit the lowest misinformation and appear to be the most robust topology. In this regime, moderate increases in connectivity shorten many geodesics in ER and WS graphs, but the heterogeneous degree distribution of BA networks concentrates information flow through a relatively small set of high-degree nodes. This may help to limit the uncontrolled spread of independent pathwise errors. Regular lattices are the worst because their long geodesic distances continue to accumulate errors.

(d) In the comparatively denser limit ($\langle k \rangle/n \gtrsim 0.14$), the hierarchy again places BA networks in the most robust position. In this regime, regular graphs also gain substantial robustness. As their connectivity increases, their highly symmetric structure begins to suppress errors more effectively. This allows them to outperform both ER and WS networks. BA networks, however, retain their apparent advantage and yield the smallest misinformation among the four classes.

VII. EFFECT OF BIASED PATHWISE ERRORS

In our model, the information that node j receives about node i accumulates stochastic errors along the shortest path of length d_{ij} . If u of the d_{ij} steps contribute positive increments and the rest contribute negative ones, the perceived state takes the form given in Eq. 3, where u follows a binomial distribution with parameters (d_{ij}, r) . The parameter r controls a directional bias: for $r = 1/2$ the noise is symmetric, whereas $r \neq 1/2$ introduces a preference for either positive or negative updates. One might expect such a bias to modify the perceived distribution by introducing skewness or broadening. However, the actual effect is far simpler: the bias induces only a uniform shift of the distribution, while its overall fluctuation structure remains unchanged.

A. Mean and fluctuation structure of the accumulated error

To make the impact of the bias explicit, we decompose the binomial variable into its mean and zero-mean fluctuation:

$$u = d_{ij}r + \delta u, \quad \overline{\delta u} = 0, \quad \text{Var}(\delta u) = d_{ij}r(1-r). \quad (27)$$

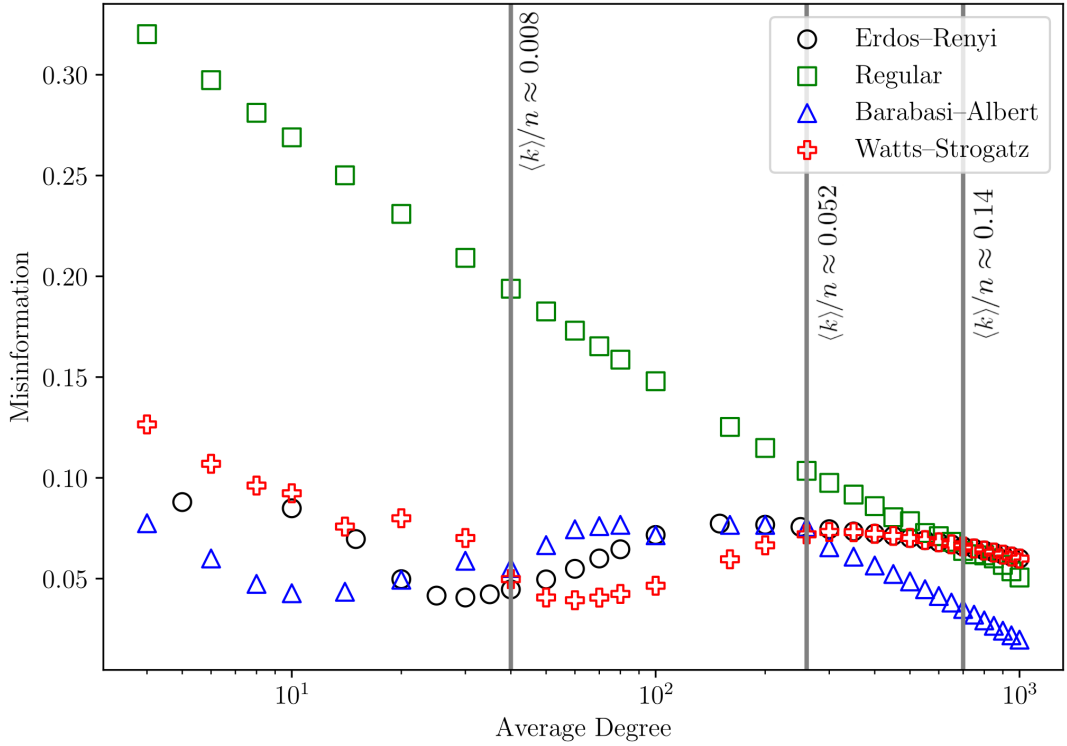


FIG. 5. **A comparison of misinformation across regular, ER, WS, and BA networks, all constructed with $n = 5000$ nodes.** Regular networks consistently exhibit the highest misinformation in the sparse to intermediate-dense regimes due to their long path lengths and absence of shortcuts. In the extremely sparse regime, ER and BA networks behave similarly, with BA showing slightly lower misinformation because early-formed hubs provide local aggregation. As connectivity increases into an intermediate (but still relatively low) range, a clear crossover emerges: WS networks achieve the lowest misinformation as they enter the small-world regime, where the introduction of a modest number of shortcuts sharply reduces characteristic path lengths while largely preserving local structure. In the intermediate-dense to dense-connected regime, BA networks outperform all other topologies, yielding the smallest misinformation among the classes considered. The WS curve shown here corresponds to a rewiring probability of $\beta = 0.1$, which lies within the small-world regime. The black solid lines represent the transition points, where $\langle k \rangle$ denotes the average degree.

This separates the two essential components of the binomial error process. The term $d_{ij}r$ represents the expected number of positive increments along the path of length d_{ij} , whereas the deviation $\delta u = u - d_{ij}r$ captures zero-mean fluctuations around this drift. Because $u \sim \text{Bin}(d_{ij}, r)$, these fluctuations have variance $d_{ij}r(1-r)$ and quantify the intrinsic randomness of path-wise error accumulation. This decomposition makes clear how the bias parameter influences information transfer: the mean shifts with r , while the fluctuation structure remains unchanged.

Substituting (27) into (3) yields the exact expression

$$\begin{aligned} X^{(j \leftarrow i)} &= X_i + \frac{1}{n-1} [2(d_{ij}r + \delta u) - d_{ij}] \\ &= X_i + \frac{d_{ij}(2r-1)}{n-1} + \frac{2}{n-1} \delta u. \end{aligned} \quad (28)$$

Equation (28) makes the structure of the propagated error explicit. The first term is a deterministic drift, proportional to $(2r-1)$ that grows linearly with the shortest-path length d_{ij} , and vanishes in the unbiased

case $r = 1/2$. The second term contains the fluctuations, proportional to δu , which remain symmetric for all values of r . Thus, the bias affects only the mean shift and leaves the fluctuation distribution—its symmetry, tails, and overall shape-unaltered, apart from the standard binomial variance $d_{ij}r(1-r)$, which is symmetric under $r \leftrightarrow (1-r)$.

B. Translation of the perceived distribution

Let $Q_0^{(j)}(x)$ denote the distribution of $X^{(j \leftarrow i)}$ in the unbiased case $r = 1/2$. From Eq. (28), the perceived value under general r can be written as

$$X^{(j \leftarrow i)}(r) = X^{(j \leftarrow i)}(1/2) + \Delta\mu_{ij}, \quad (29)$$

where the shift is

$$\Delta\mu_{ij} = \frac{d_{ij}(2r-1)}{n-1}. \quad (30)$$

The fluctuation term $2\delta u/(n-1)$ does not appear explicitly because its distribution is independent of r : the bias modifies only the mean of $X^{(j \leftarrow i)}$, while the centered binomial fluctuations remain unchanged. Thus, the effect of bias is a pure translation,

$$Q_r^{(j)}(x) = Q_0^{(j)}(x - \Delta\mu_{ij}), \quad (31)$$

meaning that each perceived value is shifted by a constant amount.

To understand why Eq. (31) preserves the functional shape of the distribution, consider the case where the true state X_i is Gaussian. The perceived value $X^{(j \leftarrow i)}$ is the sum of this Gaussian variable, a constant drift, and a centered binomial fluctuation. Because the fluctuation term is a sum of independent Bernoulli increments, it is approximately Gaussian by the central limit theorem [76]; and the sum of two Gaussian variables is Gaussian [77]. Hence the overall shape is preserved. This drift–fluctuation decomposition mirrors classical treatments of stochastic processes [78]. Equation (31) therefore shows that *bias does not deform the distribution*: it introduces no broadening, skewness, or change in shape. It generates only a uniform drift proportional to the geodesic distance and the imbalance $(2r - 1)$, while the statistical structure of the underlying fluctuations remains invariant.

C. Consequences for misinformation

The KL divergence quantifying misinformation at node j becomes

$$D_{KL}\left(P(x) \parallel Q_r^{(j)}(x)\right) = D_{KL}\left(P(x) \parallel Q_0^{(j)}(x - \Delta\mu_{ij})\right), \quad (32)$$

so the only influence of r enters through the translation $\Delta\mu_{ij}$. When the true distribution $P(x)$ is Gaussian, this dependence reduces to a simple quadratic function of the drift, since a translation of a Gaussian changes only its mean. Thus, varying the bias probability cannot generate any new qualitative behaviour in the misinformation. It shifts all perceived distributions coherently while the shapes and dispersions remain unchanged. This decomposition into a deterministic drift and a shape-preserving fluctuation term mirrors classical results for biased random walks and additive binomial noise [31, 76, 78]. Similarly, in our network setting, the bias induces only a uniform shift, without altering the form of the perceived distribution.

In the limit where the true distribution collapses to a single discrete value, the impact of non-symmetric biases ($r \neq 1/2$) remains finite. Although the drift scales as $(2r - 1)d_{ij}/(n - 1)$, the binomial error mechanism ensures that $Q^{(j)}(x)$ continues to assign nonzero probability to the true state, preserving overlap between the distributions. This prevents divergences that would otherwise arise in the continuous KL divergence between

shifted delta functions. Moreover, the normalized misinformation stays bounded because both the observed and maximum possible misinformation are evaluated over the same finite discrete state space. Hence, in the δ -limit, the effect of bias is simply a smooth and finite shift in the perceived distribution.

A key physical implication is that biased errors do not increase the uncertainty of the information flowing through the network. Instead, they produce a coherent, topology-dependent displacement of the perceived state. Consequently, systematic misinformation accumulates along longer paths, making agents consistently incorrect rather than increasingly uncertain. This mechanism aligns with phenomena observed in social systems, where groups may converge to shared but biased narratives while maintaining internal confidence [79, 80]. Similar effects appear in technological and biological settings—in distributed sensing, small measurement biases can shift global consensus without increasing estimated noise [81], and in regulatory or signaling networks, biased transmission can lead to coherent misregulation rather than merely noisier responses.

VIII. DISCUSSION & CONCLUSIONS

Our results show that misinformation in complex large networks is shaped by an interplay between geodesic structure, stochastic error accumulation, and topological organization. Rather than depending solely on density or degree, misinformation emerges from how network geometry transforms local binomial errors into global distortions. This perspective unifies the behaviour of Erdős–Rényi (ER), Watts–Strogatz (WS), and Barabási–Albert (BA) networks within a single analytical and numerical framework.

In ER networks, misinformation displays a distinctive double-peaked profile as the link probability varies. Near the percolation threshold, long geodesic chains amplify accumulated fluctuations, whereas at slightly higher densities the coexistence of extended paths and emerging cycles produces a second, weaker maximum [6, 62]. Only at high densities—where shortest paths collapse logarithmically—does misinformation sharply decrease. This behaviour highlights a general principle: misinformation is maximized when the network is sufficiently connected to propagate signals widely yet sparse enough to preserve long, error-amplifying routes.

WS networks reveal a complementary trend. A small amount of rewiring creates a narrow small-world regime in which misinformation is minimized. Sparse random shortcuts reduce path lengths dramatically while retaining strong local structure [10, 61]. This structural crossover resembles transport optimisation in disordered media [63]. Notably, empirical biological networks—neural, metabolic, genetic, and ecological—often fall precisely within this low-to-intermediate randomness range [22, 67, 82], aligning with our observation that

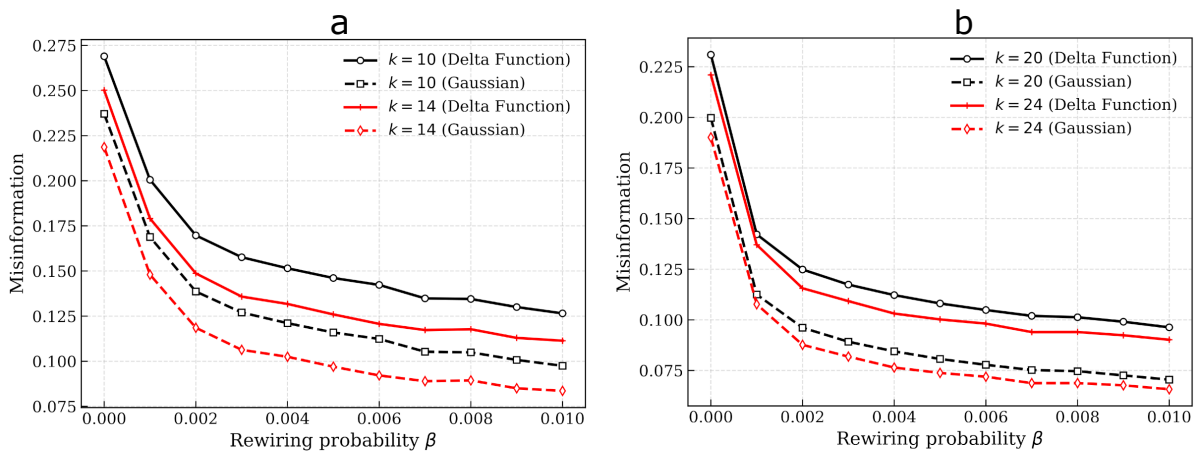


FIG. 6. **Comparison of misinformation for δ -distributed and narrow Gaussian initial states as a function of the rewiring probability β .** The Gaussian distribution is centred at the same value as the δ distribution and has a small standard deviation of 10^{-4} . The result is independent of the mean of the Gaussian distribution. Even this extremely small intrinsic variance reduces the peak misinformation compared to the δ case, indicating that broader true states partially absorb accumulated binomial fluctuations.

small-world architectures suppress global distortion.

BA networks exhibit the lowest level of misinformation both in the sparse and intermediate-density connectivity regimes. High-degree hubs act as robust integrators that shorten effective distances, dilute noise, and stabilise information flow [26, 27, 41, 66]. This result provides a quantitative explanation for the resilience of scale-free systems—heterogeneity and hub dominance inherently suppress the accumulation of pathwise errors. Although BA networks are known to facilitate rapid propagation of both information and errors due to their hub-dominated architecture [83, 84], our results show that, within a static error-accumulation model, they exhibit robustness to path induced errors. This apparent contrast between quick dynamical error propagation and suppressed misinformation is a nontrivial feature of scale-free topology. This feature highlights an interesting phenomenon that merits investigation in future work.

A central analytical contribution of this work is the demonstration that directional bias in the error process creates only a uniform drift in the perceived state, without altering the fluctuation structure. The biased process splits into an additive drift term and a shape-preserving noise term, similar to classical stochastic-process theory [76, 78]. Consequently, biased errors produce *coherent misinformation* rather than uncertainty. Our formalism connotes several observed phenomena in social systems, where groups converge to internally confident but biased narratives [79, 80]—and in technological or biological networks, where small sensor biases imbalances drive global misregulation [81].

Comparing delta-distributed and narrow Gaussian true states reveals that even minimal intrinsic stochasticity reduces achievable misinformation (consistent with Eq. 10) and smooths its dependence on connectivity

(Fig. 6). We show that an intrinsic heterogeneity in the true global state can act as a buffer to error propagation as small errors remain partly absorbed within the spread of the true state, whereas a perfectly sharp state is maximally fragile.

Overall, our findings reveal a unified physical picture: *misinformation is governed by the geometry of geodesic paths and the structure of fluctuations, and different network topologies impose distinct transformation rules on how local stochastic errors accumulate*. Scale-free networks suppress distortion through hub-dominated integration; small-world networks exploit a balance between clustering and global shortcuts; and ER networks amplify noise near structural transitions.

Our framework opens several avenues for further work. Extending the model to weighted, directed, temporal, or multilayer networks would allow the analysis of systems with richer dynamical features. Incorporating correlated or memory-dependent errors could reveal how temporal persistence modifies misinformation accumulation. From an optimisation perspective, one could search for cost-constrained rewiring strategies that will minimize global distortion or identify network modifications that maximize robustness under biased or adversarial noise. Finally, coupling this framework with agent-based dynamics or adaptive topology could shed light on how real systems evolve to balance efficiency, robustness, and misinformation suppression.

Overall, the theoretical and numerical results presented here lay a foundation for a statistical physics of information distortion in complex networks, providing both mechanistic insight and a versatile analytical toolset for future studies.

AUTHOR CONTRIBUTIONS

Archana Mukhopadhyay: Conceptualization (lead), Formal Analysis (equal), Methodology (equal), Supervision (lead), Writing- Original draft (lead). **Jens Christian Claussen:** Conceptualization (supporting), Supervision (supporting), Validation (equal). **Saikat Sur:** Formal Analysis (equal), Methodology (equal), Supervision (supporting), Writing- Reviewing and Editing (lead), Visualization (supporting). **Rohitashwa Chat-topadhyay:** Validation (equal), Visualization (lead), Data curation (lead), Writing- Reviewing and Editing (supporting).

ACKNOWLEDGEMENTS

SS acknowledges the support of the Department of Chemical and Biological Physics and AMOS at the Weizmann Institute of Science, Israel, where a significant part of this work was carried out. JCC acknowledges financial support from the EPSRC through grant EP/V048740/2. AM acknowledges support from the School of Computer Science, University of Birmingham, and the Centre for Ecological Sciences, Indian Institute of Science, Ben-

galuru, where parts of this work were conducted. His stay at the University of Birmingham was supported by the EPSRC through grant EP/V048740/2, and his stay at the Indian Institute of Science, Bengaluru, was supported by the SERB (DST, Government of India) through project no. PDF/2023/001151. AM is currently employed at M. S. Ramaiah University of Applied Sciences. RC gratefully acknowledges the generous allocation of computing resources by the Department of Theoretical Physics (DTP), Tata Institute of Fundamental Research (TIFR), along with related technical assistance from Kapil Ghadiali and Ajay Salve.

DATA AVAILABILITY STATEMENT

The data supporting the findings of this study are available from the corresponding author upon reasonable request.

CONFLICTS OF INTEREST

The authors have no conflicts to disclose.

[1] D. Krol and G. Kukla, Computing and Informatics **28**, 811–842 (2012).

[2] G. Li, S. K. S. Hari, M. Sullivan, T. Tsai, K. Pattabiraman, J. Emer, and S. W. Keckler, in *SC17: International Conference for High Performance Computing, Networking, Storage and Analysis* (2017) pp. 1–12.

[3] K. Klemm and S. Bornholdt, Proceedings of the National Academy of Sciences **102**, 18414 (2005).

[4] A. Ghoshal, N. Das, S. Das, and S. Dhar, Soc. Netw. Anal. Min. **15**, (2012).

[5] F. Nian, Y. Shi, and J. Cao, Journal of Computational Science **55**, 101438 (2021).

[6] M. Newman, *Networks: An Introduction* (Oxford University Press, Inc., USA, 2010).

[7] A.-L. Barabási and M. Pósfai, *Network science* (Cambridge University Press, Cambridge, 2016).

[8] R. Pastor-Satorras and A. Vespignani, Phys. Rev. Lett. **86**, 3200 (2001).

[9] D. Brockmann and D. Helbing, Science **342**, 1337 (2013).

[10] D. J. Watts and S. H. Strogatz, Nature **393**, 440 (1998).

[11] K. Klemm and V. M. Eguíluz, Phys. Rev. E **65**, 036123 (2002).

[12] H. C. Berg, Biophysical Journal **86**, 1643 (2004).

[13] Y. Tu, Proceedings of the National Academy of Sciences **105**, 11737 (2008).

[14] A. A. Faisal, L. P. J. Selen, and D. M. Wolpert, Nature Reviews Neuroscience **9**, 292 (2008).

[15] P. Dayan and L. F. Abbott, *Theoretical Neuroscience: Computational and Mathematical Modeling of Neural Systems* (MIT Press, Cambridge, MA, 2001).

[16] M. B. Elowitz and S. Leibler, Nature **403**, 335 (2000).

[17] M. B. Elowitz, A. J. Levine, E. D. Siggia, and P. S. Swain, Science **297**, 1183 (2002).

[18] A. Raj and A. van Oudenaarden, Cell **135**, 216 (2008).

[19] W. E. Paul, *Fundamental Immunology*, 7th ed. (Lippincott Williams & Wilkins, 2012).

[20] A.-L. Barabási and Z. N. Oltvai, Nature Reviews Genetics **5**, 101 (2004).

[21] A. Destexhe and D. Paré, Journal of Neurophysiology **81**, 1531 (1999), pMID: 10200189.

[22] U. Alon, *An Introduction to Systems Biology: Design Principles of Biological Circuits* (Chapman & Hall/CRC, 2007).

[23] A. S. Perelson and G. Weisbuch, Reviews of Modern Physics **69**, 1219 (1997).

[24] R. Medzhitov and C. A. J. Janeway, Cell **91**, 295 (1997).

[25] A. Hoffmann, A. Levchenko, M. L. Scott, and D. Baltimore, Science **298**, 1241 (2002).

[26] J. D. Han, N. Bertin, T. Hao, D. S. Goldberg, G. F. Berriz, L. V. Zhang, D. Dupuy, A. J. Walhout, M. E. Cusick, F. P. Roth, and M. Vidal, Nature **430**, 88 (2004).

[27] H. Jeong, S. P. Mason, A.-L. Barabási, and Z. N. Oltvai, Nature **411**, 41 (2001).

[28] J. C. Claussen, Physica A: Statistical Mechanics and its Applications **375**, 365 (2007).

[29] J. Kim and T. Wilhelm, Physica A: Statistical Mechanics and its Applications **387**, 2637 (2008).

[30] E. Desurvire, *Classical and Quantum Information Theory: An Introduction for the Telecom Scientist* (Cambridge University Press, 2009).

[31] T. M. Cover and J. A. Thomas, *Elements of Information Theory (Wiley Series in Telecommunications and Signal Processing)* (Wiley-Interscience, USA, 2006).

[32] D. J. C. MacKay, *Information Theory, Inference & Learning Algorithms* (Cambridge University Press, USA, 2002).

[33] A. V. Oppenheim, R. W. Schafer, and J. R. Buck, *Discrete-Time Signal Processing*, 2nd ed. (Prentice-hall Englewood Cliffs, 1999).

[34] A. E. Brouwer, A. M. Cohen, and A. Neumaier, *Distance-Regular Graphs*, 1st ed., *Ergebnisse der Mathematik und ihrer Grenzgebiete. 3. Folge, Vol. 18* (Springer-Verlag, Berlin / Heidelberg, 1989) softcover reprint 2011 ISBN 978-3-642-74343-6 / eBook ISBN 978-3-642-74341-2.

[35] B. Bollobás, “Random graphs,” in *Modern Graph Theory* (Springer New York, New York, NY, 1998) pp. 215–252.

[36] M. E. J. Newman, S. H. Strogatz, and D. J. Watts, *Phys. Rev. E* **64**, 026118 (2001).

[37] F. R. K. Chung, *Spectral Graph Theory*, CBMS Regional Conference Series in Mathematics, Vol. 92 (American Mathematical Society, 1997).

[38] P. Erdős and A. Rényi, *Publicationes Mathematicae Debrecen* **6**, 290 (1959).

[39] M. Haenggi, J. G. Andrews, F. Baccelli, O. Dousse, and M. Franceschetti, *IEEE Journal on Selected Areas in Communications* **27**, 1029 (2009).

[40] M. E. J. Newman, *Proceedings of the National Academy of Sciences* **98**, 404 (2001).

[41] A.-L. Barabási and R. Albert, *Science* **286**, 509 (1999).

[42] R. Albert, H. Jeong, and A.-L. Barabási, *Nature* **401**, 130 (1999).

[43] B. Bollobás, *Random Graphs*, 2nd ed., Cambridge Studies in Advanced Mathematics (Cambridge University Press, 2001).

[44] S. Wasserman and K. Faust, *Social Network Analysis: Methods and Applications*, Structural Analysis in the Social Sciences (Cambridge University Press, 1994).

[45] X.-Y. Li, *Wireless Communications and Mobile Computing* **3**, 119 (2003).

[46] S. Song, P. J. Sjöström, M. Reigl, S. Nelson, and D. B. Chklovskii, *PLoS Biol* **3**, e68 (2005).

[47] S. Lefort, C. Tomm, J.-C. Floyd Sarria, and C. C. Petersen, *Neuron* **61**, 301 (2009).

[48] R. Perin, T. K. Berger, and H. Markram, *Proceedings of the National Academy of Sciences* **108**, 5419 (2011).

[49] F. Chung and L. Lu, *Proceedings of the National Academy of Sciences* **99**, 15879 (2002).

[50] M. E. J. Newman, *SIAM Review* **45**, 167 (2003).

[51] R. Albert and A.-L. Barabási, *Rev. Mod. Phys.* **74**, 47 (2002).

[52] M. Girvan and M. E. J. Newman, *Proceedings of the National Academy of Sciences* **99**, 7821 (2002).

[53] R. Albert, *J Cell Sci* **118**, 4947 (2005).

[54] E. Ravasz, A. L. Somera, D. A. Mongru, Z. N. Oltvai, and A.-L. Barabási, *Science* **297**, 1551 (2002).

[55] J. M. Montoya and R. V. Solé, *Journal of Theoretical Biology* **214**, 405 (2002).

[56] L. A. N. Amaral, A. Scala, M. Barthélémy, and H. E. Stanley, *Proceedings of the National Academy of Sciences* **97**, 11149 (2000).

[57] V. Latora and M. Marchiori, *Phys. Rev. Lett.* **87**, 198701 (2001).

[58] O. Sporns and J. D. Zwi, *Neuroinformatics* **2**, 145 (2004).

[59] M. D. Humphries and K. Gurney, *PLOS ONE* **3**, 1 (2008).

[60] M. Kaiser and C. C. Hilgetag, *Phys. Rev. E* **69**, 036103 (2004).

[61] S. H. Strogatz, *Nature* **410**, 268 (2001).

[62] A. Barrat, M. Barthélémy, and A. Vespignani, *Dynamical Processes on Complex Networks* (Cambridge University Press, 2008).

[63] S. N. Dorogovtsev, A. V. Goltsev, and J. F. F. Mendes, *Rev. Mod. Phys.* **80**, 1275 (2008).

[64] M. E. J. Newman and D. J. Watts, *Phys. Rev. E* **60**, 7332 (1999).

[65] M. E. J. Newman, C. Moore, and D. J. Watts, *Phys. Rev. Lett.* **84**, 3201 (2000).

[66] R. Albert, H. Jeong, and A.-L. Barabási, *Nature* **406**, 378 (2000).

[67] H. Jeong, B. Tombor, R. Albert, Z. N. Oltvai, and A.-L. Barabási, *Nature* **407**, 651 (2000).

[68] A. Wagner and D. A. Fell, *Proceedings of the Royal Society B: Biological Sciences* **268**, 1803 (2001).

[69] V. M. Eguíluz, D. R. Chialvo, G. A. Cecchi, M. Baliki, and A. V. Apkarian, *Phys. Rev. Lett.* **94**, 018102 (2005).

[70] E. Bullmore and O. Sporns, *Nature Reviews Neuroscience* **10**, 186 (2009).

[71] P. Hagmann, L. Cammoun, X. Gigandet, R. Meuli, C. J. Honey, V. J. Wedeen, and O. Sporns, *PLoS Biol* **6**, e159 (2008).

[72] D. S. Modha and R. Singh, *Proceedings of the National Academy of Sciences* **107**, 13485 (2010).

[73] M. P. van den Heuvel and H. E. Hulshoff Pol, *European Neuropsychopharmacology* **20**, 519 (2010).

[74] T. I. Lee, N. J. Rinaldi, F. Robert, D. T. Odom, Z. Bar-Joseph, G. K. Gerber, N. M. Hannett, C. T. Harbison, C. M. Thompson, I. Simon, J. Zeitlinger, E. G. Jennings, H. L. Murray, D. B. Gordon, B. Ren, J. J. Wyrick, J.-B. Tagne, T. L. Volkert, E. Fraenkel, D. K. Gifford, and R. A. Young, *Science* **298**, 799 (2002).

[75] M. M. Babu, N. M. Luscombe, L. Aravind, M. Gerstein, and S. A. Teichmann, *Current Opinion in Structural Biology* **14**, 283 (2004).

[76] W. Feller, *An Introduction to Probability Theory and its Applications, Volume 1* (J. Wiley & Sons: New York, 1968).

[77] S. C. Port, *SIAM Review* **28**, 275 (1986).

[78] N. G. Van Kampen, *Stochastic processes in physics and chemistry*, 3rd ed. (Elsevier, Amsterdam, 2008).

[79] M. D. Vicario, A. Bessi, F. Zollo, F. Petroni, A. Scala, G. Caldarelli, H. E. Stanley, and W. Quattrociocchi, *Proceedings of the National Academy of Sciences* **113**, 554 (2016).

[80] C. R. Sunstein, *Going to Extremes: How Like Minds Unite and Divide* (Oxford University Press, 2009).

[81] R. Olfati-Saber, J. A. Fax, and R. M. Murray, *Proceedings of the IEEE* **95**, 215 (2007).

[82] O. Sporns and J. D. Zwi, *Neuroinformatics* **2**, 145 (2004).

[83] M. Barthélémy, A. Barrat, R. Pastor-Satorras, and A. Vespignani, *Phys. Rev. Lett.* **92**, 178701 (2004).

[84] S. Wang, Y. Deng, and Y. Li, *Royal Society Open Science* **5**, 181137 (2018).

Appendix A: Mean-field estimate of misinformation for a Gaussian true distribution

Let $P(x)$ denote a normalized probability density function and $Q(x)$ be another probability density that differs

from $P(x)$ by a small perturbation $\Delta(x)$, i.e.,

$$Q(x) = P(x) + \Delta(x), \quad (\text{A1})$$

where $\Delta(x)$ satisfies the normalization constraint

$$\int dx \Delta(x) = 0. \quad (\text{A2})$$

The Kullback–Leibler divergence is defined as

$$D_{\text{KL}}(P\|Q) = \int dx P(x) \ln \frac{P(x)}{Q(x)}. \quad (\text{A3})$$

Substituting Eq. (A1) into Eq. (A3), we obtain

$$\begin{aligned} D_{\text{KL}}(P\|Q) &= \int dx P(x) \ln \left(\frac{P(x)}{P(x) + \Delta(x)} \right) \\ &= - \int dx P(x) \ln \left(1 + \frac{\Delta(x)}{P(x)} \right). \end{aligned} \quad (\text{A4})$$

Assuming $|\Delta(x)/P(x)| \ll 1$, we expand the logarithm in a Taylor series $\ln(1+u) = u - \frac{u^2}{2} + \frac{u^3}{3} - \dots$. Retaining terms up to second order, Eq. (A4) gives

$$D_{\text{KL}}(P\|Q) \approx - \int dx P(x) \left[\frac{\Delta(x)}{P(x)} - \frac{1}{2} \left(\frac{\Delta(x)}{P(x)} \right)^2 \right]. \quad (\text{A5})$$

Distributing $P(x)$ inside the integrand,

$$D_{\text{KL}}(P\|Q) \approx - \int dx \Delta(x) + \frac{1}{2} \int dx \frac{\Delta(x)^2}{P(x)}. \quad (\text{A6})$$

By the normalization condition Eq. (A2), the linear contribution in Eq. (A6) vanishes identically. Hence,

$$D_{\text{KL}}(P\|Q) \approx \frac{1}{2} \int dx \frac{\Delta(x)^2}{P(x)}. \quad (\text{A7})$$

For a fixed ordered pair of nodes (i, j) , the cumulative error accumulated along the shortest path of length d_{ij} arises from d_{ij} independent Bernoulli trials with bias r . Each trial contributes an error of magnitude $\pm 1/(n-1)$. The mean and variance of the total error are therefore

$$\begin{aligned} m_{ij} &= (2r-1) d_{ij} \frac{1}{n-1} \approx (2r-1) c_{ij}, \quad 0 < c_{ij} := \frac{d_{ij}}{n} < 1, \\ v_{ij} &= 4r(1-r) d_{ij} \left(\frac{1}{n-1} \right)^2 \approx 4r(1-r) \frac{c_{ij}}{n}, \end{aligned}$$

where the approximations hold in the large-network limit $n \rightarrow \infty$. The variance v_{ij} vanishes as $\mathcal{O}(1/n)$, implying that fluctuations around the mean shift are negligible asymptotically.

If distances from node j are approximately homogeneous across the network, we may replace c_{ij} by a node-dependent mean value c_j , yielding $m_{ij} \approx m_j = (2r-1)c_j$.

Neglecting fluctuations of order $\mathcal{O}(n^{-1/2})$, the perceived distribution at node j becomes

$$Q^{(j)}(x) = \frac{1}{n} \sum_i P(x - m_{ij}) \approx P(x - m_j). \quad (\text{A8})$$

Since $0 < c_j < 1$ and $|2r-1| \leq 1$, we have $|m_j| < 1$.

In a mean-field description, the empirical distribution of rescaled distances c_j converges to a density $\rho(c)$ with finite moments. Introducing $\alpha := 2r-1 \in [-1, 1]$, we write $m_j = \alpha c_j$, with $|m_j| < 1$. Assuming self-averaging of distance statistics in the large- n limit, node-dependent moments converge to network-wide constants,

$$\overline{m}_j \rightarrow \overline{m}, \quad \overline{m_j^2} \rightarrow \overline{m^2}.$$

Accordingly, the perceived distribution becomes asymptotically independent of j , and we write $Q_j(x) \approx Q(x)$.

The node-averaged perceived distribution is then

$$\begin{aligned} Q(x) &= \frac{1}{n} \sum_j Q^{(j)}(x) = \int_0^1 P(x - m(c)) \rho(c) dc \\ &= P(x) - \overline{m} P'(x) + \frac{\overline{m^2}}{2} P''(x) + \mathcal{O}(m^3), \end{aligned} \quad (\text{A9})$$

where $\overline{m^k} = \int_{c=0}^1 (ac)^k \rho(c) dc$. Defining $\Delta(x) = Q(x) - P(x)$ yields

$$\Delta(x) = -\overline{m} P'(x) + \frac{\overline{m^2}}{2} P''(x) + \mathcal{O}(m^3). \quad (\text{A10})$$

For a Gaussian true distribution $P(x) = \mathcal{N}(0, \sigma^2)$, the derivatives satisfy

$$\frac{P'(x)}{P(x)} = -\frac{x}{\sigma^2}, \quad \frac{P''(x)}{P(x)} = \frac{x^2}{\sigma^4} - \frac{1}{\sigma^2}. \quad (\text{A11})$$

Using the quadratic approximation to the KL divergence, valid when $|\Delta(x)| \ll P(x)$, we obtain from (A7)

$$\begin{aligned} D_{\text{KL}}(P\|Q) &\approx \frac{1}{2} \int dx \frac{\Delta(x)^2}{P(x)} \\ &= \frac{\overline{m}^2}{2\sigma^2} + \frac{\overline{m^2}^2}{4\sigma^4} + \mathcal{O}(m^6). \end{aligned} \quad (\text{A12})$$

Averaging over nodes yields the network-level misinformation

$$I = \frac{1}{n} \sum_j D_{\text{KL}}(P\|Q^{(j)}) \approx \frac{A}{2\sigma^2} + \frac{B}{4\sigma^4}, \quad (\text{A13})$$

where $A = \overline{m}^2$ and $B = \overline{m^2}^2$ depend on the distance statistics of the network and satisfy $0 < A, B < 1$ for any connected graph.